Inner Control Method and Frequency Regulation of a DFIG Connected to a DC-Link

G. D. Marques, *Senior Member, IEEE,* M. F. Iacchetti, *Member IEEE*

***Abstract*—An inner loop for the control and frequency regulation of the Doubly-Fed Induction Generator connected to a dc link through a diode bridge on the stator is presented in this paper. In this system, the stator is directly connected to the dc link using a diode bridge and the rotor is fed by only a PWM ~~electronic~~ converter. Because the system uses less one PWM inverter, the cost of power electronics is reduced in this system when compared with the DFIG connected to an ac grid. Additionally, it uses a diode bridge that is much less expensive. The application in mind is for dc networks as dispersed generation grids and microgrids. These networks use several elements that should work together. Usually, these elements are each other connected by power electronic devices in a common dc link. This paper presents a control system for the inner control loop in order to regulate the torque and the stator frequency. Simulation and experimental results show that the system works acceptably and is able to keep the stator frequency near the rated value of the machine.**

***Index Terms*— Doubly-fed Induction Generator, Dc link, control, Dc Micro-grids.**

NOMENCLATURE

General

e, E	Dynamical, steady-state stator electromotive force.
i, I	Dynamical, steady-state stator or rotor current.
I_m	Magnetizing current.
k_s	Gain of the synchronization loop.
k_p, k_i	Parameters of the PI controller.
L_s, M	Stator and mutual inductance.
n_{12}	Stator-rotor turns ratio.
u, U	Dynamical, steady-state voltage.
r_s	Stator resistance.
δ	Field orientation error.
ε_s	Speed error.
$\gamma_{s\psi}$	Position of the stator flux vector.
γ_m	Electrical position of the rotor.
ω_b	Rated or base frequency.
ω_m	Mechanical speed.
ω_s^*	Reference frequency.
ω_s	Stator frequency.
ψ	Flux linkage

Superscripts

^	Estimated value.
*	Reference value.

Subscripts

d, q	Variables on a common moving reference frame.
s, r	Stator or rotor quantities.
R	Variable relative to the Γ equivalent circuit

G. D. Marques is with INESC-ID, IST, University of Lisbon, Portugal, email: gil.marques@tecnico.ulisboa.pt.
M.F. Iacchetti is with the Dipartimento di Energia, Politecnico di Milano, Milan, Italy, email: matteo.iacchetti@polimi.it.

I. INTRODUCTION

TODAY there is a considerable interest in using dc networks in several cases. Examples are dispersed generation applications and microgrids. In such applications, there are several systems that should be connected together using power electronics as tools for improving efficiency. The use of dc versus ac links can be advantageous, because less power electronics can be used. Moreover no reactive power is circulating in dc networks.

A microgrid can be defined as a part of a distribution network with multiple distributed generation as renewable energy sources like photovoltaic panels, small wind turbines etc., and storage systems. Most commonly used energy storage devices in a microgrid are batteries, supercapacitors, flywheels, and fuel cells. These systems, with local loads, can be disconnected from the upstream network under emergency conditions [1]-[2].

To allow the power connection between distributed generation sources, storages and loads, a direct current (dc) link or an alternating current (ac) link can be used. Today, these different devices that should work together are power electronics controlled and each one of these converters needs a dc link [3]-[11]. If the same dc link is used, considerable savings can be obtained.

The Doubly-Fed Induction Generator (DFIG) is a well-known machine. It has been applied to wind power extraction plants working in generator mode with adjustable speed and in hydroelectric pumping stations working alternatively in generator and motoring modes. Its main advantage is that, for a small range of speed adjustment, it needs power electronics devices rated to a fraction of the rating power of the wind turbine. In this system, the stator is directly connected to the network, and the rotor is connected to the network by an ac/dc/ac frequency converter [12], [13].

Most of the applications of the DFIG use it connected to the ac mains. This can now be considered as mature technology. Recent advances are dealing with the sensorless operation [14]-[16]. There are also other applications where the DFIG is used in standalone operation [17]-[22]. In this case there is no ac network that imposes the stator frequency, hence this should be regulated by the control system.

This paper analyzes a control system for a DFIG connected to a dc link by a diode bridge on the stator and through a single PWM inverter in the rotor [23]-[24]. Also by comparing the typical costs of the power electronics and the costs of the generator in a wind turbine [25], this layout brings considerable benefits because only a PWM ac/dc converter is necessary, and the diode rectifier is very cheap.

The system is suitable for applications as dc networks, microgrids, and for the integration of various electrical sources and storages on a common dc link.

Since there are no special requirements about the quality of the stator voltage, the purpose of the control system is to control the DFIG torque and to regulate the stator frequency near the rated frequency of the DFIG. A control technique based on the detection of the orientation error and on the adjustment of the d-axis rotor current has been proposed in [24]. However only preliminary results have been shown in [24]: no theoretical approach to design the control parameters nor a deep discussion of the performances have been provided. These aspects are developed in the present paper. An improved method to force the field orientation on the stator flux linkage and to control the frequency and the power is discussed, specifically aimed to a DFIG connected to a dc link by a diode rectifier.

Section II presents the layout of the system. The modeling and a brief steady state analysis are presented in Section III, considering the operation with field orientation. Section IV is devoted to the description of the control system as well as to its theoretical analysis, including rules to set the regulator parameters. Simulations in Section V and experimental results in Section VI show that the system can be applied in microgrids operating as generator coupled to small wind turbines.

II. System Layout

As shown in Fig. 1, the stator of the DFIG is connected to a dc link by a diode bridge rectifier: the same dc link feeds the rotor converter, so that only a dc/ac PWM converter is needed. Opposite positive directions are used for the stator and rotor powers and currents. The rectifier allows only the operation as generator: the shaft torque is considered negative. A lower delimitation for the value of the DFIG turn-ratio n_{12} which allows the rotor inverter and the rectifier to share the same dc link is given in [24].

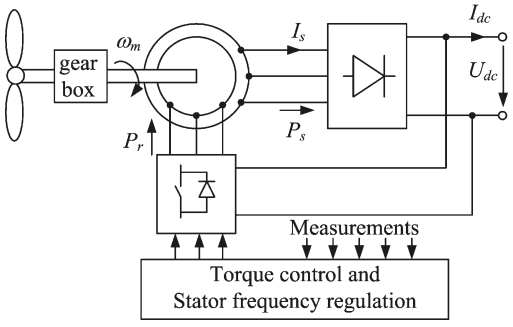

Fig. 1 Structure of the DFIM-DC. Diode bridge on the stator, PWM converter on the rotor.

In the system in Fig. 1, the magnetizing current is provided only by the rotor. Thus, the rated magneto-motive force (MMF) of the rotor should be higher than that one of the stator. This implies an increase of the inverter rated power which will be discussed in Section VI. Since the slip induction machine is symmetric, the roles of the stator and rotor windings are interchangeable. Thus, a DFIG with a rotor rated MMF lower that the stator one can be used all the same by connecting the diode rectifier to the rotor and by feeding the stator by the PWM converter.

III. Modeling and Analysis at Steady State

The analysis is performed by using the Γ equivalent circuit shown in Fig. 2. In case of a current-controlled rotor, the relevant equations in a frame oriented with the stator flux are [12]:

$$u_{sd} = -r_s i_{sd} + e_{sd} = -r_s i_{sd} + \frac{d\psi_s}{dt} \quad , \qquad (1)$$

$$u_{sq} = -r_s i_{sq} + e_{sq} = -r_s i_{sq} + \psi_s \frac{d\gamma_{s\psi}}{dt} \quad , \qquad (2)$$

$$\psi_s = L_s\left(-i_{sd} + i_{Rd}\right) \quad , \quad 0 = -i_{sq} + i_{Rq} \quad , \qquad (3)$$

where

$$i_{Rd} = \left(M/L_s\right) i_{rd} \quad , \quad i_{Rq} = \left(M/L_s\right) i_{rq} \quad . \qquad (4)$$

Since the stator is connected to a diode rectifier, the stator currents and voltages are not sinusoidal. To have an insight into the operation of the system, the steady state equivalent circuit in Fig. 2 can be used by considering the fundamental harmonic.

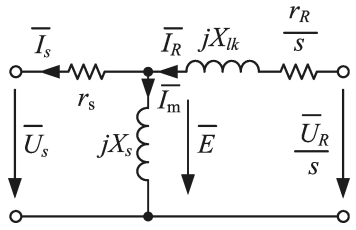

Fig. 2 Γ equivalent circuit of the induction machine at steady-state.

Generally, even when the rectifier works with a noticeable overlapping angle due to the ac equivalent inductance, the phase shift between the first harmonic of the ac current and of the ac voltage immediately across the rectifier is low [24], [26]. Moreover, the difference between the first harmonics of the stator electromotive force (EMF) E and of the stator voltage U_s is minimal, because it is due only to the voltage drop across r_s. This means that E and U_s are almost in phase. Thus it can be concluded that I_s is almost aligned to E, i.e. the $I_{sd} \approx 0$ (in average). It should be noticed that in a synchronous machine such an argument would not hold, because the q axis would be aligned to the internal EMF, not to the stator EMF, so that an additional phase shift due to the armature inductance should be taken into account. Some simulative and test results will confirm this assumption.

Fig. 3 shows the approximate phasor diagram (with $I_{sd} \approx 0$) related to the first harmonic components and supposes that the DFIG is vector-controlled by using a frame oriented with the stator flux linkage: this control technique with some modifications will be used also in this paper.

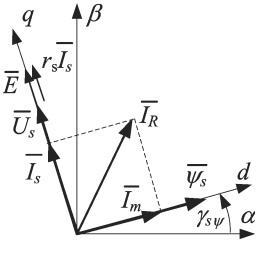

Fig. 3 Steady state phasor diagram considering ϕ_1=0.

When the field orientation is achieved, the rectifier determines $i_{sd} \approx 0$ and the whole stator current, i.e. also the stator power and the electromagnetic torque, can be controlled acting on i_{Rq}. Moreover, by considering the stator flux at steady state, (2) becomes

$$u_{sq} + r_s i_{sq} = e_{sq} = \omega_{s\psi} \psi_s \approx \omega_{s\psi} L_s i_{Rd} \,. \qquad (5)$$

As it will be deeply shown in Section IV, (5) states the possibility to use i_{Rd} in order to change the relation between the stator frequency ω_s and the stator voltage, and to control the stator frequency.

IV. Control Scheme and Analysis

A. Objectives.

In this paper, it is assumed that the purpose of this system is to be connected to a dc link with a given constant dc voltage. In ac-grid-connected DFIGs the frequency of the stator is imposed by the ac network: DFIGs are optimized for the rated frequency, which should be guaranteed. Because there is now a diode bridge, the frequency of the stator is no more imposed by an ac mains: the consequence is the necessity of a frequency regulation in this system in order to match the rated frequency of the DFIG. This condition guarantees that the rated power is reached with appropriate value of the stator flux. A similar requirement arises in stand-alone DFIGs connected to ac loads. However, in the application here considered, no ac loads are fed by the DFIG: thus, also distorted stator voltages can be tolerated.

Similarly to grid connected DFIGs, another aim of the system is the control of the torque or of the speed in order to match the optimal operation conditions of the wind turbine for a given wind speed [23].

In order to achieve the control of the frequency and of the torque, the field oriented control (FOC) is used: suitable rotor current set points i_{rd}^* and i_{rq}^* in a proper reference frame (dq) are realized by the rotor converter.

B. Reference frame orientation for the control system

Field orientation is based on reference frame transformations associated with a space vector. Typically, in the control of DFIGs, the reference frame is aligned to the stator flux linkage, which guarantees the decoupling of the torque and reactive power control chains. Being the control system acting on the rotor, and being γ_s the reference position for the reference frame where the control is performed, the transformation angle is the slip position angle γ_{sr} defined as:

$$\gamma_{sr} = \gamma_s - \gamma_m \,. \qquad (6)$$

The angle γ_m is the rotor position angle. Because γ_m can be measured, or estimated using sensorless methods, the problem of reference frame determination reduces to determine γ_s.

As referred before, in the control of DFIGs, γ_s should be the stator flux position angle $\gamma_{s\psi}$. However, in the considered case, $\gamma_{s\psi}$ is not directly used. In fact, it is necessary to control the average frequency of the stator flux, because it is not guaranteed *a priori*. In ac stand alone DFIGs [21], the orientation along the stator flux linkage can be achieved by using as stator flux angle the reference angle obtained as integral of the reference frequency and by forcing to zero the q-axis stator flux component. However, a rigid frequency is not advantageous here, because, due to the constant voltage dc bus, the system tends to behave as a parallel of two voltage sources decoupled by the small r_s, causing highly discontinuous stator currents.

The first proposed approach is shown in Fig. 3. The reference angle γ_s^* is obtained integrating the set-point frequency ω_s^*. Then γ_s^* is corrected with ε_p that is a smooth function of the difference δ between the desired stator flux position γ_s and the actual stator flux position $\gamma_{s\psi}$. In this work, $\gamma_{s\psi}$ is calculated by a stator flux estimator based on the integration of the stator EMF [28]. Alternatively, the Luenberger observer in [21] could be used. If δ is kept small, one can conclude that the system works approximately in field orientation. The low-pass filter is implemented to smooth the variations in δ. The angle γ_s (i.e. γ_s^* corrected by ε_p) is used in the frame transformations.

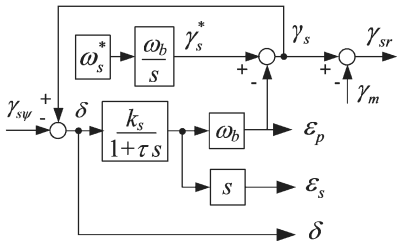

Fig. 3. System to obtain the reference frame control angle.

The parameters of the system in Fig. 3 are the gain k_s and the time constant τ. Since from Fig. 3 $\delta = \gamma_s - \gamma_{s\psi}$, the angle δ can be considered as an orientation error in the FOC.

The position error and speed errors are defined in the block diagram of Fig. 3 as

$$\varepsilon_p = \gamma_s^* - \gamma_s \quad \text{(rad)} \quad , \quad \varepsilon_s = \omega_s^* - \omega_s \quad \text{(p.u.)} \,. \qquad (7)$$

The position error ε_p is of no importance, whereas its derivative ε_s measures the stator reference frame speed error with respect to the set point. It is related with the stator frequency error that can be defined as $e_f = w_s^* - w_{s\psi}$. A detailed study leads to the conclusion that ε_f is similar to ε_s.

C. Analysis and improvement of the synchronization loop

Considering the block diagram of Fig. 3, it can be written:

$$\gamma_s = \gamma_s^* - \frac{\omega_b k_s}{1 + s\tau} \delta \,. \qquad (8)$$

Subtracting $\gamma_{s\psi}$ to both terms in (8), results:

$$\gamma_s - \gamma_{s\psi} = \delta = \gamma_s^* - \gamma_{s\psi} - \frac{\omega_b k_s}{1 + s\tau} \delta \,. \qquad (9)$$

From (9) the following transfer function is deduced:

$$\frac{\delta}{\left(\gamma_s^* - \gamma_{s\psi}\right)} = \frac{1 + s\tau}{1 + \omega_b k_s + s\tau} \,. \qquad (10)$$

In order to obtain a low order model of the whole synchronization loop, (2), (3-1) with $i_{sd} \approx 0$ and (5) are used:

$$\psi_s = L_s i_{Rd} = M i_{rd} \quad , \quad \omega_s = \frac{e_{sq}}{\psi_s} = \frac{u_{sq} + r_s i_{Rq}}{\psi_s} . \qquad (12)$$

Since fast rotor current controllers are assumed, the feedback rotor currents can be considered equal to the set-point values. However, the orientation error δ must be taken into account in the analysis. Hence, the actual d-axis (magnetizing) rotor current is related to the reference rotor currents by:

$$i_{Rd} = \frac{M}{L_s} i_{rd} = \frac{M}{L_s} \left(i_{rd}^* \cos\delta - i_{rq}^* \sin\delta \right) . \qquad (13)$$

Linearizing (12) and (13) around a steady state point (subscript 0) where $\omega_{s\psi 0} = (U_{sq0} + r_s I_{Rq0})/\psi_{s0}$ and neglecting the variations on i_{rq} due to adjustments of δ yields

$$\Delta\psi_s(s) = M \left(\cos\delta_0 \Delta i_{rd}^* - \sin\delta_0 \Delta i_{rq}^* - k_1 \Delta\delta \right) \quad , \qquad (14)$$

$$\Delta\omega_{s\psi} = \frac{\Delta e_{sq}}{\psi_{s0}} - \frac{\omega_{s\psi 0}}{\psi_{s0}} \Delta\psi_s \cong \frac{\Delta u_{sq}}{\psi_{s0}} - \frac{\omega_{s\psi 0}}{\psi_{s0}} \Delta\psi_s \ , \qquad (15)$$

where

$$k_1 = I_{rd0}^* \sin\delta_0 + I_{rq0}^* \cos\delta_0 \quad . \qquad (16)$$

Equations (14) and (15) are represented by the block diagram in Fig. 6 which is a closed loop ~~if $k_1 \approx 0$~~ only if $k_1 \neq 0$. At very low load, i.e. when $I_{Rq0} \approx 0$ so that $k_1 \approx 0$, the system operates in open loop: in such a condition it cannot annihilate the frequency error, and the resulting frequency depends only on the operation conditions through (12-2) and (16). Besides, Fig. 6 shows that the steady state orientation error introduces a coupling between the dynamics of the torque-producing reference current component Δi_{rq}^* and the synchronization loop. This fact suggests the introduction of a PI controller which acts on i_{rd}^* in order to annihilate the orientation error δ and to obtain the proper field orientation. The improved scheme is shown in Fig. 7.

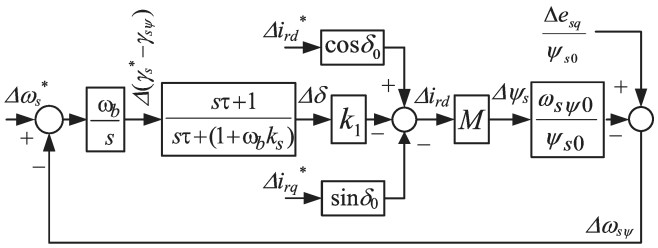

Fig. 4 Block scheme for the synchronizing loop: the term ω_b/s allows to express $\gamma_s^* - \gamma_{s\psi}$ in (10) in terms of the frequency error $\omega_s^* - \omega_{s\psi}$.

The transfer function of the PI in p. u. variables is defined as:

$$i_{rd}^* = -\left(k_p + \frac{\omega_b k_i}{s} \right) \delta = -\frac{k_p s + \omega_b k_i}{s} \delta \ . \qquad (17)$$

Due to the PI, $\delta_0 = 0$ and $k_1 = I_{rq0}$: the resulting block diagrams are shown in Fig. 8 and 9.

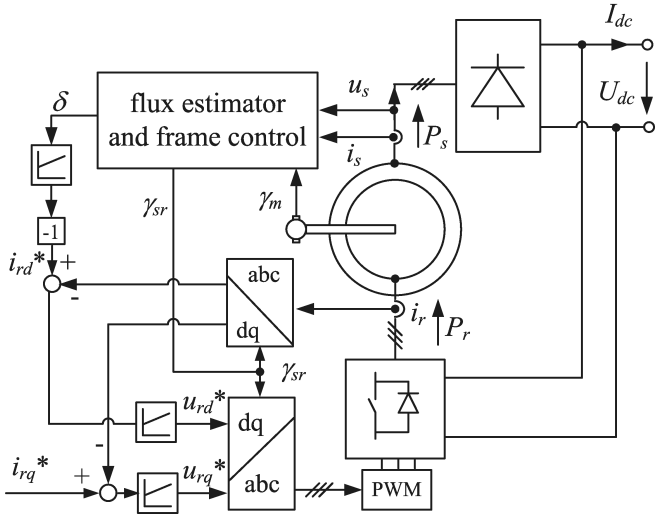

Fig. 5 Control structure using a low pass filter in the synchronizing loop and an additional PI controller to adjust the d-axis reference rotor current.

According to Fig. 8 and due to the additional PI controller, the system always operates in closed loop conditions, even at no load (i.e. when $I_{Rq0} \approx 0$). The PI regulator not only tracks the reference frequency in any condition and with the desired dynamics: it also annihilates the orientation error δ.

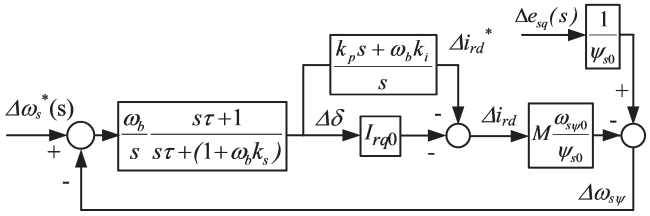

Fig. 6 Block diagram for the synchronizing loop including the PI.

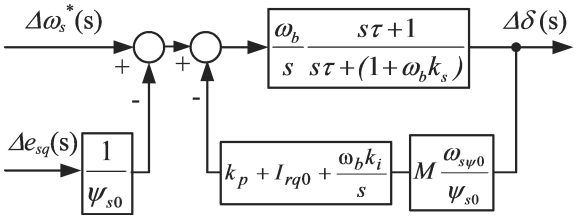

Fig. 7 Modified Block diagram for the synchronizing loop with the PI.

The closed loop transfer function can be obtained performing some manipulations:

$$\Delta\delta(s) = \frac{s(1+s\tau)\omega_b}{D(s)} \left(\Delta\omega_s^*(s) - \frac{1}{\psi_{s0}} \Delta e_{sq}(s) \right) , \qquad (18)$$

where the denominator $D(s)$ is

$$D(s) = s^3\tau + s^2 \left(1 + \omega_b k_s + (k_p + I_{rq0}) K \tau \right) + sK \left(k_p + I_{rq0} + k_i \omega_b \tau \right) + \omega_b k_i K \qquad (19)$$

In (19), the auxiliary constant K is defined as

$$K = \omega_b M \frac{\omega_{s\psi 0}}{\psi_{s0}} . \qquad (20)$$

The transfer function (18) has two zeros and three poles. One of the zeros is located on the origin. Since $\omega_s^* = (s/\omega_b)\,\gamma_s^*$ and $\omega_s = (s/\omega_b)\,\gamma_{s\psi}$, due to (7) and (10) the speed error is:

$$\Delta\varepsilon_s(s) = \omega_b k_s \frac{s^2}{D(s)}\left(\Delta\omega_s^*(s) - \frac{1}{\psi_{s0}}\Delta e_{sq}(s)\right) . \quad (21)$$

The transfer functions (18) and (21) represent the dynamics of the system. This is a linear three-order system with four parameters to adjust. Using the final value theorem, it can be concluded that k_i should be different of zero to allow a zero steady state error in both functions. The parameter k_p can be small to avoid big variations on the reference d-axis current. So, an acceptable solution is to set k_p =0. The other parameters should be adjusted to obtain the required behavior.

The dominant real pole s_3 can be computed by supposing $s \to 0$ in (19) so that the terms in s^3 and s^2 are neglected. In this way, an approximation of (19) by a first order polynomial near the lower frequencies is used:

$$s_3 = -\frac{1}{I_{rq0}/\omega_b k_i + \tau} \cong -\frac{1}{\tau} . \quad (22)$$

The pole in (22) cancels with the corresponding zero in (18), thus (18) behaves as a second order system. This allows an analytic study using approximations $\omega_b k_s >> 1$ and k_p=0 in (18).

D. System stability analysis

The local system stability can be analyzed considering the block diagram of Fig 9. Using the simplifications assumed above, the two poles of the system can be computed as:

$$s_{1,2} = -\frac{\omega_b}{2}\left(\frac{k_s}{\tau} + I_{rq0}M\frac{\omega_{s\psi 0}}{\psi_{s0}}\right) \pm \frac{\omega_b}{2}\sqrt{\left(\frac{k_s}{\tau} + I_{rq0}M\frac{\omega_{s\psi 0}}{\psi_{s0}}\right)^2 - 4k_i M\frac{\omega_{s\psi 0}}{\psi_{s0}}} . \quad (23)$$

Being k_i and I_{rqo} always positive, the system is always stable because the real part is always negative.

E. Determination of the integral gain

The poles, computed analytically, can be placed on the complex plane to be complex conjugate at 45º. This guarantees good dynamics for both variables δ and ε_s. After some manipulations, imposing poles placed at 45º, it results

$$k_i = \frac{\psi_{s0}}{2M\omega_{s\psi 0}}\left(\frac{k_s}{\tau} + I_{rq0}M\frac{\omega_{s\psi 0}}{\psi_{s0}}\right)^2 , \quad (24)$$

$$s_{1,2} = \frac{\omega_b}{2}\left(\frac{k_s}{\tau} + I_{rq0}M\frac{\omega_{s\psi 0}}{\psi_{s0}}\right)(-1 \pm j) . \quad (25)$$

The value of k_i, which affects the damping of the poles $s_{1,2}$, depends on k_s/τ and on the operating conditions: Fig. 10 shows responses for three different values of k_s/τ. A good response is obtained using k_s/τ = 3.

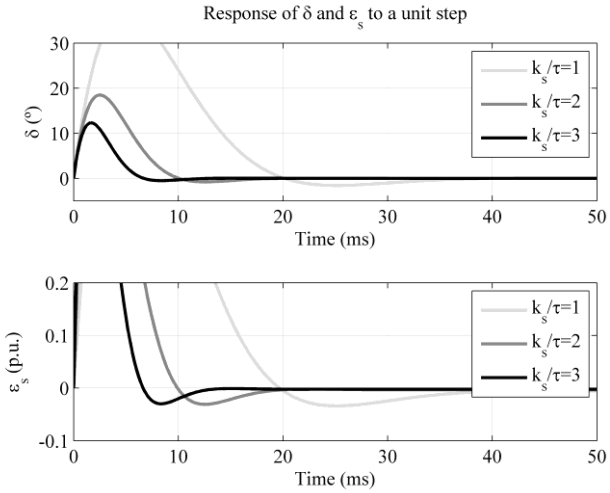

Fig. 8 Response to a unit step for complex conjugate poles and three values for k_s/τ .

Since I_{rq0} (i.e. the load) increases the damping, an acceptable response is obtained if the k_i parameter is computed using the constant value I_{rq0}=0 in (24). Anyway, (24) could be also implemented as a gain scheduling for k_i , in order to mitigate the effect of the particular operating point on the damping of the system.

V. Simulation Results

Preliminarily, the behavior of the proposed control scheme has been assessed by some simulations which are hereafter presented. The parameters of the DFIG are reported in the Appendix.

Using the theory described above, the relation k_s/τ=3 was adopted using k_s=1.5 and τ=0.5sec. The dc link voltage was set at 0.67 p. u. in order to have a lower flux level with respect to the rated value. The reason of this choice will be explained in Section VI.

A. Using only the reference frame control angle determination system.

Figs. 11 show the results obtained in open loop using only the reference frame angle determination system.

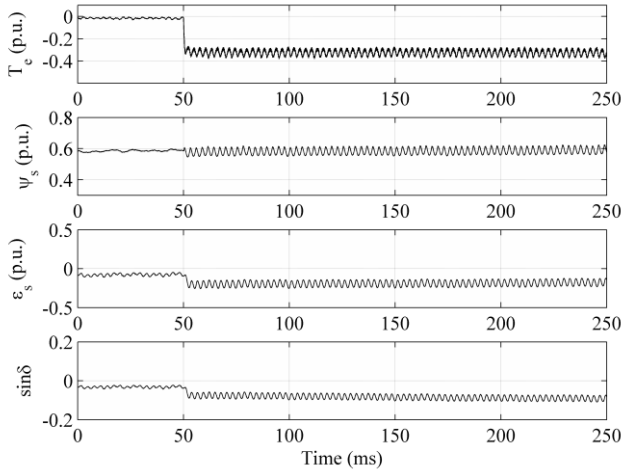

Fig. 9 Torque, stator flux, frequency error and sinδ.

The *d*-axis rotor current component is fixed at 0.5 p. u. At

the instant t=50 ms, a step on the reference q-axis rotor current is set. Fig 11 shows the torque T_e, the stator flux ψ_s, the speed error ε_s and sinδ. According to this, the frequency error ε_s in Fig. 11 is not zero. The peak-to-peak ripple in the torque waveform is less than 0.1 p.u..

B. *Using the d-axis rotor current adjustment system.*

By enabling the adjustment of the direct rotor current reference i_{rd}^*, the performances improve considerably. A value of k_i given by (24) with I_{rq0}=0 was used. The stator and rotor currents, on the reference frame defined by γ_s, during a step of the reference rotor current i_{rq}^* are reported in Fig. 12: the average d-axis stator current i_{sd} at steady state is very close to zero and confirms the assumption in Section III. Fig. 13 shows that the torque ripple is comparable with that one of the first approach. Moreover here sinδ≈0 i.e. the field orientation is achieved. Also the average frequency error in Fig. 13 decreases to zero (i.e. the frequency now is 50 Hz) and the stator flux tends to the expected value related to the U_{dc}. The response of the torque takes some time to establish in steady state according to the dynamics of the stator flux.

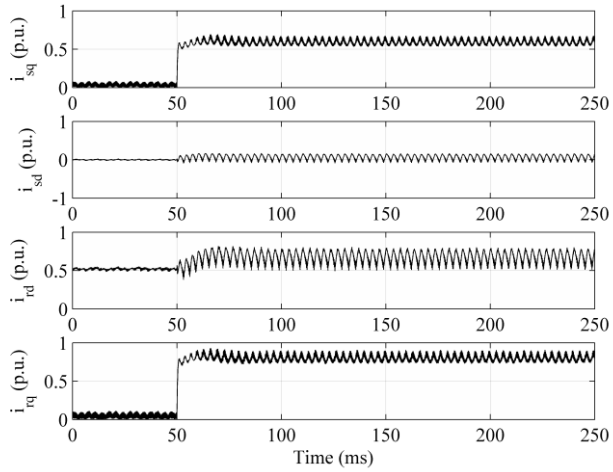

Fig. 10 Stator and rotor currents in closed loop.

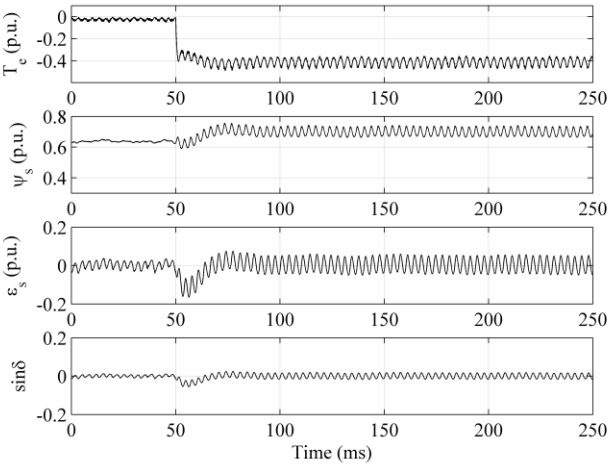

Fig. 11. Torque, stator flux, frequency error and sinδ.

VI. Additional Control and Operation Issues

In order to evaluate the feasibility of an industrial system, some additional control issues are shortly discussed.

A. *Effect of voltage dips in the DC-grid*

The response to a voltage dip down to 0.5 p. u. is presented in Fig. 14: U_{dc} decreases from 1 p. u. to 0.5 p. u. at t=100 ms and raises again after 200 ms. This result was obtained at rated voltage and load. Conversely to the ac-grid connected DFIG the response of the stator flux present zero-sequence components only in the first instants. In these instants the VSI loses control, but the free-wheeling diodes of the rotor converter clamp the rotor voltages to the dc link voltage protecting the VSI from over-voltages. So, the overvoltage of the conventional DFIG connected to the ac mains does not occur. Nevertheless the system must be protected with respect to the over-currents. After the loss of control, that lasts about one stator cycle, the system restores the current control, because the rotor d-axis current is decreased and adjusted to the new conditions. The system has an excellent response to the increase stage that occurs at t=200ms.

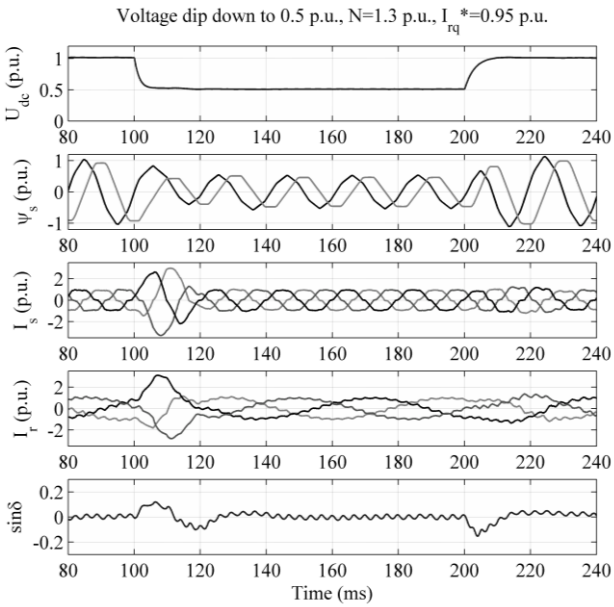

Fig. 12 Response to a voltage dip down to 0.5 p. u.

B. *Effect of the harmonics*

Fig. 13 showed that the torque is affected by some ripple: its main component is at 300 Hz and it is due to the 5th and 7th harmonics in the flux and in the currents. Such a ripple could be attenuated by using two different approaches. A first method consists in using a q-axis reference current given by $i_{rq}^* = -T_e/\psi_s$. However, i_{rq}^* would be affected by a noticeable 6th harmonic, and a good tracking capability of the current controllers would be needer, in order to achieve an effective compensation of the torque ripple. PI controllers would be inadequate: they could be supported by additional resonant controllers tuned at 300 Hz [22]. Anyway, this method does not reduce the harmonic content of the currents.

Alternatively, a twelve-pulse rectifier could be used instead of a simple three-phase bridge. Such a configuration is obtained by using two sets of stator windings electrically shifted by 30 deg. Fig. 15 compares the stator currents and the torque in the two configurations, namely: six and twelve-pulse rectifiers. The same average torque and the same global stator MMF are considered in the comparison. It can be noticed that the twelve-pulse system allows to achieve a

considerable reduction of both the torque ripple and the distortion of the stator currents. The THD of the stator currents are …….

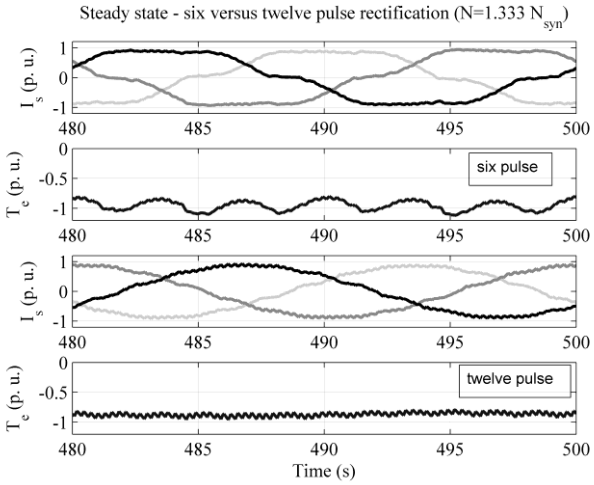

Fig. 135 Twelve-pulse rectification curves. Stator currents and equivalent three-phase current, rotor currents and torque.

C. *Rating of the inverter*

By considering the magnetization current supplied only through the rotor, and the sinusoidal operation, the inverter rated power $A_{inv\,(DC)}$ can be deduced by the diagram in Fig. !

$$\frac{A_{inv(DC)}}{A_S} = I_r \sqrt{\left(|s|_{\max} E + X_{kr} I_{rd}\right)^2 + \left(X_{kr} I_{rq}\right)^2} \quad , \quad ()$$

where I_r =1 p.u., I_{rd} = I_m , I_{rq} =$(1-I_m^2)^{1/2}$ p.u. can be assumed. In an ac-grid connected DFIG with the whole magnetization current supplied by the grid, the rating of the rotor converter $A_{inv\,(AC)}$ is still provided by (), where I_{rd} =0, I_r =I_{rq} =$(1-I_m^2)^{1/2}$ p.u.. Thus, the ratio $A_{inv\,(DC)}/A_{inv\,(AC)}$ is

$$\frac{A_{inv(DC)}}{A_{inv(AC)}} = \sqrt{\frac{\left(|s|_{\max} E + I_m\right)^2 + \left(X_{kr}\left(1-I_m^2\right)\right)^2}{\left(1-I_m^2\right)\left(\left(|s|_{\max} E\right)^2 + \left(X_{kr}\left(1-I_m^2\right)\right)^2\right)}} \approx 1.39$$

where I_m= 0.35 p.u. and $|s|_{max}$= 0.33 have been supposed. The effect of the current harmonics could be taken into account by the coefficient $(1+THD_{Ir}^2)^{1/2}$, where THD_{Ir}^2 is the total harmonic distortion of the rotor currents.

VII. Experimental Results

Some experimental tests have been performed using a 3.2 kW slip-ring induction machine, Fig. 14, where a photo of the experimental setup is presented. The slip ring machine is connected to a DC Machine that works as a motor feeding it with mechanical power. This machine is operated using a rheostat to adjust the field current , being the armature winding is regulated using a VARIAC and a diode bridge. In this way the speed is adjusted accordingly. The torque is adjusted using the system described in this paper. The dc-link, regulated to 200 V, is obtained using the DC network of the laboratory. It consists of an induction machine and a 40 kW dc generator placed in the basement of the laboratory. The control algorithm is implemented in a Microchip dsPIC30F4011. To obtain experimental results in real time, four PWM output channels with simple RC filters were used. The actual rotor position is measured by an encoder with a 4096 step resolution [27]. Because the rated stator voltage is 3 times higher than the rated voltage of the rotor, a step down transformer (380 V to 220 V) was used between the stator and the diode bridge. The transformer introduces an additional equivalent stator leakage about 10% of the total leakage of the induction machine. The machine parameters are given in the Appendix.

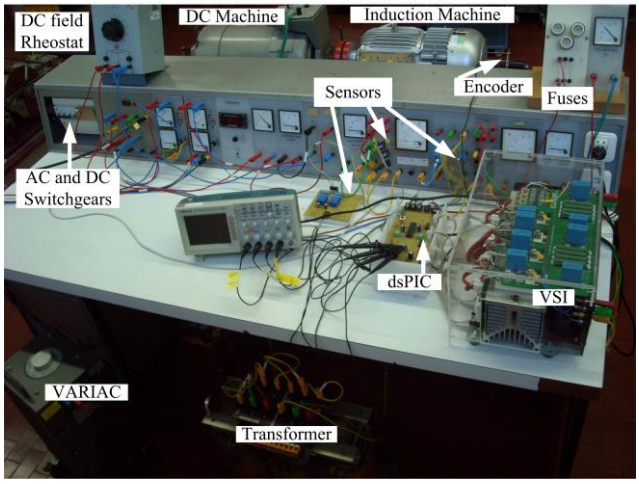

Fig. 14 Experimental setup.

Since the rated power of the rotor is smaller than the stator rated power, a lower flux with respect to the rated value is used for this experimental validation. A value near 0.67 p. u. was chosen. All results were obtained using k_s=1.5 and τ=0.5 s resulting k_s/τ =3.

A. *Using only the reference frame control angle determination system.*

Fig. 14 shows the waveforms of the *d*-axis rotor current, of the stator voltages and of sinδ when a step on the *d*-axis rotor current reference is imposed. Because this step is relatively small, the final voltage obtained is smaller than the voltage necessary to start the conduction of the diode bridge. The machine is working at no-load. One can see that the voltage waveforms are almost sinusoidal as expected. Their frequency is almost 50 Hz. It is possible to conclude that the voltage response has good behavior being fast and without undesired transients.

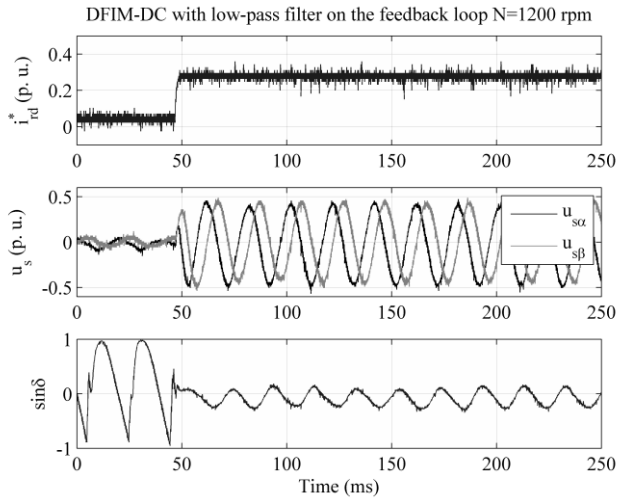

Fig. 15 Response to a step on the d-axis rotor current at no-load.

Fig. 15 shows a different transient for a step on the *q*-axis rotor current. The system is working with constant *d*-axis rotor current reference (0.52 p. u.), and, at t=50 ms there is a step on the *q*-axis rotor reference current from 4% to 80%. Since, sinδ is not null, the system is not working in field orientation and the frequency is not 50 Hz.

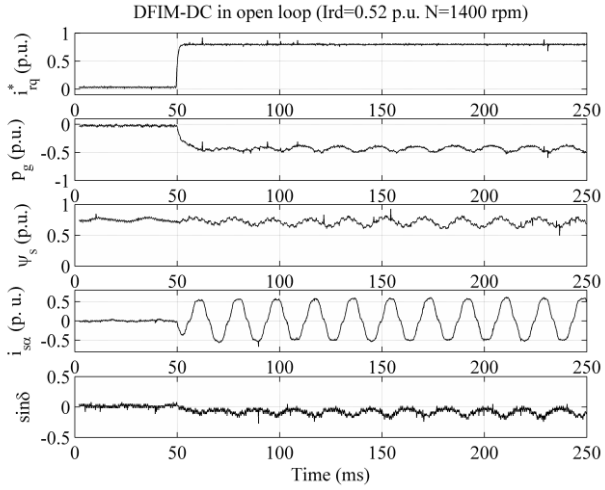

Could you add a trace with Isd? (only in this case)

Fig. 16 Response to a step on q-axis rotor reference current. The d-axis rotor reference current component is constant (i_{dr}^* =0.52 p.u.)

B. Results in closed loop

According to the scheme in Fig. 5, now the *d*-axis rotor reference current is no longer a free input, because it is adjusted using an integral controller. Figs. 16-17 show the behavior during a transient similar to that one in Fig. 15.

Here the quantity sinδ is maintained at zero thanks to the adjustment of the *d*-axis rotor current reference, thus the frequency is 50 Hz as desired. Different results were obtained using a higher value for k_i (see Fig. 17): In this case, the damping of the conjugate poles in (23) decreases and an oscillatory behavior is found, as the theory in Section IV-C predicts. Fig. 18 collects some results referred to different values of the mechanical speed and shows that the dynamical behavior depends only slightly on the speed. Fig. 19 shows some steady state waveforms: it can be concluded that the waveforms have a relatively small harmonic content. It is also possible to verify that the phase shift between the voltage and the current is small, as supposed in the section III-B.

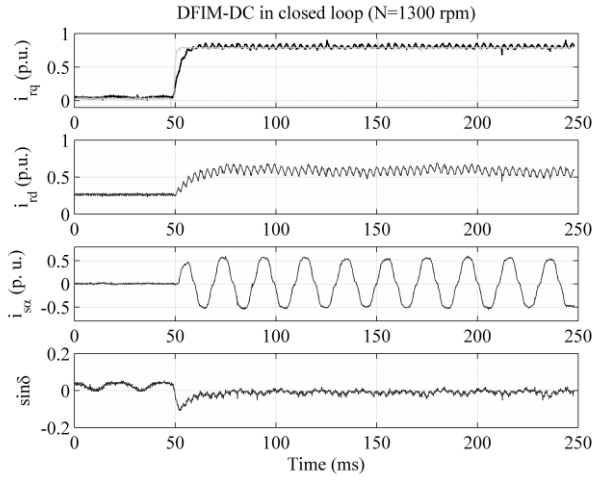

Fig. 17 Response to a step on i_q with control of d-axis reference current component using also the adjustment of the d-axis rotor current reference. (k_i =1.27).

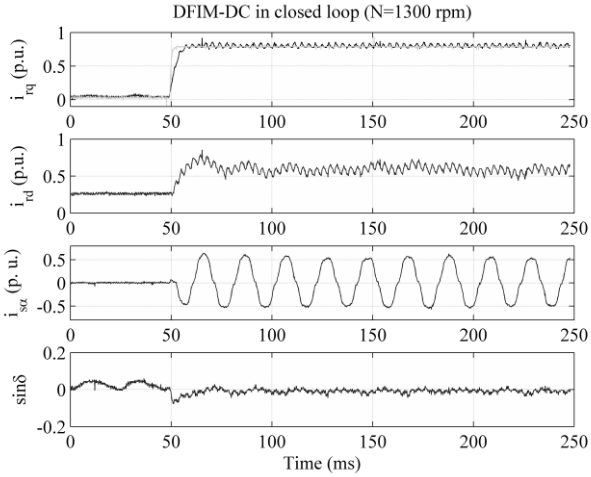

Fig. 18 Response to a step on i_q with the adjustment of the d-axis rotor current reference. (k_i =3.18). The higher k_i decreases the damping in (23) causing oscillations.

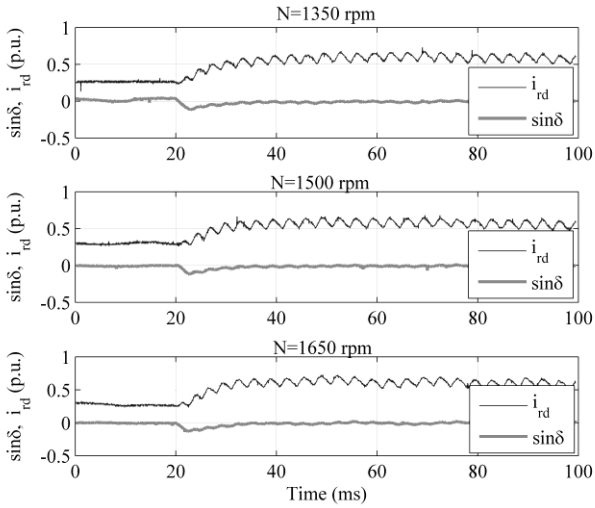

Fig. 19 Influence on the mechanical speed on the response in transients similar to Fig. 17 (k_i =1.27)

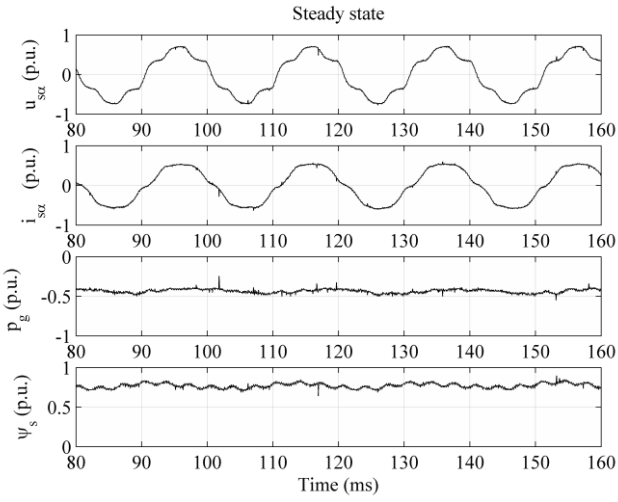

Fig. 20 Steady state waveforms after a step on *q*-axis rotor reference current.

VIII. CONCLUSION

The paper presents a control method for the DFIG connected to a dc link through a diode rectifier on the stator windings. Simulation and experimental results show that it is possible

to drive the stator flux at the rated frequency of the machine using a simple controller that adjusts the rotor *d*-axis current reference in order to annihilate the orientation error. The method converges to the field orientation and the steady state frequency error is zero. A good dynamics is achieved in the electromagnetic torque. The waveforms of the stator current are not sinusoidal, because the presence of the diode bridge, but have acceptable harmonic content. In order to decrease the torque ripple, an advanced current control could be developed, for instance by resonant controllers. However, the industrial application of this system could be implemented using a twelve-pulse rectifier, which reduces not only the torque ripple but also the harmonic content in the currents.

ACKNOWLEDGEMENTS

This work was supported by national funds through FCT – Fundação para a Ciência e a Tecnologia, under project PEst-OE/EEI/LA0021/2013.

APPENDIX

Parameters of the 3.2 kW machine

Induction Machine: stator 380 V, 8.1 A, rotor 110 V, 19 A, 3.2 kW, four poles, 1400 rpm, L_s = 1.5 p.u., M = 1.13 p.u., r_s = 0.06 p.u., r_r = 0.05 p.u..

REFERENCES

[1] S. Chowdhury, S.P. Chowdhury and P. Crossley, "Microgrids and Active Distribution Networks". *IET Renewable Energy*, series 6, The Institution of Engineering and Technology, 2009.

[2] J. A. Peças Lopes, C. L. Moreira, A. G. Madureira, "Defining Control Strategies for MicroGrids Islanded Operation*" IEEE Trans. on Power Systems*, vol. 21, no. 2, pp 916-924, May 2006.

[3] F. Blaabjerg, Z. Chen and S. B. Kjaer, "Power Electronics as Efficient Interface in Dispersed Power Generation System", *IEEE Trans. Power Electron*., vol. 19, no. 5, pp.1184 -1194, 2004

[4] F. Blaabjerg, R. Teodorescu, M. Liserre and A. V. Timbus, "Overview of Control and Grid Synchronization for Distributed Power Generation Systems", *IEEE Trans. Ind. Electron.*, vol. 53, no. 5, pp.1398 -1409 2006.

[5] D. Salomonsson and A. Sannino, "Low-voltage DC Distribution System for Commercial Power Systems with Sensitive Electronic Load", *IEEE Trans. Power Del*., vol. 22, no. 3, pp.1620 -1627, 2007.

[6] K. Kurohane, T. Senjyu, Y. Yonaha, A. Yona, T. Funabashi and C. H. Kim, "A distributed DC Power System in an Isolated Island", *in Proc. IEEE Int. Symp. Ind. Electron*. pp.1-6, 2009.

[7] P. Karlsson and J. Svensson, "DC Bus Voltage Control for a Distributed Power System", *IEEE Trans. Power Electron*., vol. 18, no. 6, pp.1405 -1412, 2003.

[8] Y. Ito, Y. Zhongqing and H. Akagi, "DC Microgrid Based Distribution Power Generation System", *Proc. IPEMC*, pp.1740 - 1745, 2004.

[9] R. T. Pinto, P. Bauer, S.F. Rodrigues, E. J. Wiggelinkhuizen, J. Pierik, B. Ferreira, "A Novel Distributed Direct-Voltage Control Strategy for Grid Integration of Offshore Wind Energy Systems Through MTDC Network" *IEEE Trans. on Ind. Electron.*, vol. 60, no. 6, pp. 2429-2441, June 2013.

[10] Ali Shamsnia, Mostafa Parniani, "A New Cost-Effective Wind Farm Structure with HVDC Link Preserving Technical Advantages of Advanced offshore Winf Farms" *in International Conference on Renewable Energies and Power Quality (ICREPQ'13*) Bilbao, Spain, 20 to 23 March 2013, Renewable Energy and Power Quality Journal No. 11, March 2013.

[11] H. Kakigano, Y. Miura, T. Ise and R. Uchida, "DC Micro-grid for Super High Quality Distribution—System Configuration and Control of Distributed Generations and Energy Storage Devices", *Proc. IEEE Power Eng. Soc. Conf*., pp.1 -7, 2006.

[12] W. Leonard, *Control of Electrical Drives*, 2nd ed. New York: Springer- Verlag, 1996.

[13] R. Pena, J. C. Clare, and G. M. Asher, "Doubly fed Induction Generator Using Back-to-Back PWM Converters and its Application to Variable-Speed Wind-Energy Generation", *Proc. Inst. Elect. Eng.– Elect. Power Appl.*, vol. 143, pp. 231-241, May 1996.

[14] R. Cárdenas, R. Pena, J. Clare, G. Asher, J. Proboste "MRAS Observers for sensorless control of Doubly-Fed Induction Generators," *IEEE Trans. Power Electron.*, vol. 23, no.3, , pp. 1075 – 1084, May 2008.

[15] G. D. Marques, D. M. Sousa, "Air-gap power vector based sensorless method for DFIG control without flux estimator", *IEEE Trans. Ind. Electron*., vol. 58, no. 10, pp. 4717-4726, Oct. 2011.

[16] F. Castelli-Dezza, G. M. Foglia, M. F. Iacchetti, R. Perini, "A MRAS Observer for Sensorless DFIM Drives with Direct Estimation of the Torque and Flux Rotor Current Components," *Trans. Power Electron*., vol. 27, no. 5, pp. 2576-2584. May 2012.

[17] G. Iwansky and W. Koczara, "DFIG-based power generation system with UPS function for variable-speed applications," *IEEE Trans. Ind. Electron*., vol. 55, no. 8, pp. 3047–3054, Aug. 2008.

[18] G. Iwanski and W. Koczara, "Sensorless direct voltage control of the stand-alone slip-ring induction generator" *IEEE Trans. on Ind. Electron.,* Vol. 54, No. 2. Apr. 2007, pp.1237-1239.

[19] R. Peña, R. Cardenas, E. Escobar, J. Clare, P. Wheeler, "Control System for Unbalanced Operation of Stand-Alone Doubly Fed Induction Generators." *IEEE Trans. Ener. Conv*., Vol. 22, No. 2, pp.544-545, June 2007.

[20] A.K. Jain, V.T. Ranganathan, "Wound Rotor Induction Generator With Sensorless Control and Integrated Active Filter for Feeding Nonlinear Loads in a Stand- Alone Grid", *IEEE Trans. on Ind. Electron.,* vol. 55. issue 1., pp: 218-228, Jan. 2008.

[21] D. Forchetti, G. Garcia, M. I. Valla, "Adaptive Observer for Sensorless Control of Stand-Alone Doubly Fed Induction Generator", *IEEE Trans. on Ind. Electronics*, vol. 56, no. 10, pp. 4174 – 4180, Oct. 2009.

[22] Van-Tung Phan, Hong-Hee Lee, "Control strategy for harmonic elimination in stand-alone DFIG applications with nonlinear loads," *IEEE Trans. Pow. Electron*, vol. 26, no. 9, pp. 2662-2675, Sept. 2011.

[23] Nisa Yu, Heng Nian and Yu Quan, "A Novel DC Grid connected DFIG System with Active Filter Based on Preditive Current Control" *in Electrical Machines and systems ICEMS 2011 international conference* 22-23 Aug 2011.

[24] G. D. Marques, M. F. Iacchetti, "Control Method of the DFIG Connected to a DC Link Through a Diode Bridge" APPECC2013 Conference Beijing, July 12-14, 2013.

[25] M. I. Blanco, "The economics of wind energy," *Renewable and Sustainable En. Rev.*, vol. 13, pp. 1372-1382, 2009.

[26] Bleijs, J. A. M. "Continuous conduction mode operation of three-phase diode bridge rectifier with constant load voltage", *IEE Proc. Electr. Power Appl.*, 2005, 152, (2), pp. 359-368.

[27] G. D. Marques, D. M. Sousa, "Stator Flux Active Damping Methods for Field-Oriented Doubly Fed Induction Generator", IEEE Trans. Energy Convers., vol. 27, no. 3, , pp. 799-806, September 2012.

[28] G. D. Marques, V. F. Pires, S. Sousa, D. M. Sousa, "A DFIG sensorless rotor position detector based on a hysteresis controller", *IEEE Trans. Energy Convers.*, vol. 26, no. 1, pp. 9-17, March 2011.

BIOGRAPHIES

G. D. Marques (M'95, SM'12) was born in Benedita, Portugal, on March 24, 1958. He received the Dipl. Ing., and Ph.D. degrees in electrical engineering from the Technical University of Lisbon, Lisbon, Portugal in 1981 and 1988, respectively.

Since 1981, he has been with the Instituto Superior Técnico, University of Lisbon, where he teaches power systems in the Department of Electrical and Computer Engineering. He has been an Associate Professor since 2000. He is also a Researcher at INESC-ID. His research interests include electrical machines, static power conversion, variable-speed drive and generator systems, harmonic compensation systems and distribution systems.

Matteo F. Iacchetti (M'10) received the Ph.D. in electrical engineering from the Politecnico di Milano, Milano, in 2008.

Currently he occupies a post doctoral position with the Dipartimento di Energia of the Politecnico di Milano. His main interests are design, modelling and control of electrical machines.